# Formation Control for Fixed-Wing UAVs Modeled with Extended Unicycle Dynamics that Include Attitude Kinematics on SO(m) and Speed Constraints

Christopher Heintz and Jesse B. Hoagg

Abstract—We present a formation-control algorithm for agents with extended unicycle dynamics that include orientation kinematics on SO(m), first-order speed dynamics, and a hard constraint on speed. The desired interagent positions are expressed in a leader-fixed coordinate frame, which is aligned with and rotates with the leader's velocity vector. Thus, the desired interagent positions vary in time as the leaderfixed frame rotates. We assume that each agent has relativeposition feedback of its neighbor agents, where the neighbor sets are such that the interagent communication (i.e., feedback) structure represents an undirected and connected graph. We also assume that at least one agent has access to a measurement its position relative to the leader. The analytic result shows that the agents converge to the desired relative positions with the other agents and the leader, and we provide sufficient conditions to ensure that each agent's speed satisfies the speed constraints. We also present an experiment with 3 fixed-wing unmanned air vehicles (UAVs) that demonstrates the leader-fixed formationcontrol algorithm.

#### I. Introduction

Autonomous multi-vehicle systems (e.g., multi-agent systems of fixed-wing UAVs) have a variety applications such as distributed sensing [1], cooperative surveillance [2], precision agriculture, and search and rescue. For formation control, each agent typically relies on sensing or interagent communication to determine necessary feedback information (e.g., interagent positions). Then, each agent uses this feedback information in combination with feedforward information (e.g., external commands, mission objectives) to accomplish tasks such as collision avoidance, cohesion, guidance, and velocity matching.

Consensus algorithms have been extended to address cohesion and collision avoidance (e.g., [3]–[7]). These approaches force agents into a predetermined formation by specifying the desired relative position between pairs of agents. Other examples of formation control algorithms include [8]–[18]. Surveys of multi-agent formation-control methods are presented in [19]–[21]. Experimental demonstrations of formation-control algorithms include [2], [14], [22]–[29]. In particular, [2], [24], [26], [27] present formation-control experiments with fixed-wing UAVs. Simulation results on formation-control for fixed-wing UAVs are also provided in [29]–[33].

This paper addresses formation control in a leader-fixed frame for agents with extended unicycle dynamics that include orientation kinematics on SO(m), first-order speed dynamics,

C. Heintz and J. B. Hoagg are with the Department of Mechanical Engineering, University of Kentucky, Lexington, KY, USA. (e-mail: cmhe234@g.uky.edu, jesse.hoagg@uky.edu).

This work is supported in part by the National Science Foundation (CNS-1932105, OIA-1539070) and the National Aeronautics and Space Administration (NNX15AR69H) through the NASA Kentucky Space Grant.

and a hard speed constraint. Related models are used in [10], [14], [26], [30], [32]–[36], but these models, with the exception of [33], do not include orientation kinematics on SO(m), and do not include a speed constraint.

In this paper, the desired interagent positions are expressed in a leader-fixed coordinate frame, which is aligned with the leader's velocity vector. The leader can be a physical agent or a virtual agent. The algorithm in this paper applies to formations where: i) the neighbor sets are such that the interagent communication structure represents an undirected and connected graph; ii) at least one agent has access to a measurement its position relative to the leader; and iii) each agent also has feedforward of the leader's velocity, acceleration, and orientation and its first two derivatives. In some applications, the higher-order feedforward signals (e.g., acceleration and angular acceleration) can be neglected. The main analytic result shows that for almost all initial conditions, the agents converge to the desired relative positions with the other agents and the leader. We note that topological constraints associated with SO(m) prevent global convergence using a continuous time-invariant control [37]. Furthermore, we provide sufficient conditions to ensure that each agent's speed satisfies the speed constraints.

We also present an experiment demonstrating the leader-fixed formation-control algorithm with a group of fixed-wing UAVs. To implement the leader-fixed formation-control algorithm, we use middle-loop controllers to determine the roll, pitch, and throttle commands based on the controls computed by the formation-control algorithm. An onboard Pixhawk autopilot provides inner-loop attitude stabilization, failsafe functionality, and telemetry. Each UAV obtains feedback of its position and velocity from its onboard Pixhawk autopilot and transmits this feedback to other UAVs over a secure ad-hoc wireless network. This experiment demonstrates the leader-fixed formation-control method using three fixed-wing UAVs.

# II. PROBLEM FORMULATION

Let the positive number n be the number of agents, and define the agent index set  $\mathcal{I} \triangleq \{1,2,\ldots,n\}$ . Define  $\mathcal{P} \triangleq \{(i,j) \in \mathcal{I} \times \mathcal{I} : i \neq j\}$ , which is the set of ordered pairs. Unless otherwise stated, all statements that involve the subscript i are for all  $i \in \mathcal{I}$ , and all statements that involve the subscripts i and j are for all  $(i,j) \in \mathcal{P}$ .

For clarity of presentation, we first develop the extended unicycle model in three-dimensional space. Thus, for the moment, let m=3. Let E be an inertial frame (e.g., the Earth frame), and let  $o_{\rm E}$  be the origin of E. Let  $o_i$  be the location of the ith agent (e.g., the location of the ith vehicle's

center of mass). The position of  $o_i$  relative to  $o_{\rm E}$  is  $\overrightarrow{q_i}$ , and the ith agent's position  $\overrightarrow{q_i}$  is resolved in E as  $q_i \triangleq \overrightarrow{q_i}|_{\rm E}$ . The velocity of  $o_i$  relative to  $o_{\rm E}$  with respect to E is  $\overrightarrow{p_i} \triangleq^{\rm E} \cdot \overrightarrow{q_i}$ . Let  $B_i$  be a frame that is fixed to  $o_i$  such that  $\overrightarrow{p_i}$  resolved in  $B_i$  is given by  $\overrightarrow{p_i}|_{B_i} = s_i v_i$ , where  $v_i \in \mathbb{R}^m$  is a unit vector, and for all  $t \geq 0$ ,  $s_i(t) \in \mathbb{R}$  is the speed of the ith agent, which is subject to the constraint  $s_i(t) \in \mathcal{S}_i \triangleq (\underline{s_i}, \overline{s_i})$ , where  $0 < \underline{s_i} < \overline{s_i}$ . Let  $R_i : [0, \infty) \to \mathrm{SO}(m)$  be the rotation matrix from  $B_i$  to E. Thus, the ith agent's velocity  $\overrightarrow{p_i}$  resolved in E is  $\overrightarrow{p_i}|_{\rm E} = s_i R_i v_i$ , which implies that

$$\dot{q}_i(t) = s_i(t)R_i(t)v_i,\tag{1}$$

where  $t \geq 0$ ;  $q_i(t) \in \mathbb{R}^m$ ,  $s_i(t) \in \mathcal{S}_i$ , and  $R_i^{\mathrm{T}}(t) \in \mathrm{SO}(m)$  are the position, speed, and orientation of the *i*th agent; and  $q_i(0) \in \mathbb{R}^m$  is the initial condition. Note that  $R_i v_i$  is the unit vector in the direction of the velocity  $\dot{q}_i$ . The speed and orientation of the *i*th agent satisfy

$$\dot{s}_i(t) = f_i(s_i(t), R_i(t)) + g_i(s_i(t), R_i(t))u_i(t), \quad (2)$$

$$\dot{R}_i(t) = R_i(t)\Omega_i(t),\tag{3}$$

where  $t \geq 0$ ;  $u_i : [0, \infty) \to \mathbb{R}$  and  $\Omega_i : [0, \infty) \to \operatorname{so}(m)$  are the control inputs;  $s_i(0) \in \mathcal{S}_i$  and  $R_i(0) \in \operatorname{SO}(m)$  are the initial conditions; and  $f_i : \mathcal{S}_i \times \operatorname{SO}(m) \to \mathbb{R}$  and  $g_i : \mathcal{S}_i \times \operatorname{SO}(m) \to \mathbb{R$ 

Let  $o_{\rm g}$  be the location of the leader, which can be a physical agent (e.g., a vehicle) or a virtual agent. The position of  $o_{\rm g}$  relative to  $o_{\rm E}$  is  $\overrightarrow{q_{\rm g}}$ , and the leader's position  $\overrightarrow{q_{\rm g}}$  is resolved in E as  $q_{\rm g} \triangleq \overrightarrow{q_{\rm g}}|_{\rm E}$ , which is assumed to be twice continuously differentiable. The velocity of  $o_{\rm g}$  relative to  $o_{\rm E}$  with respect to E is  $\overrightarrow{p_{\rm g}} \triangleq^{\rm E} \overrightarrow{q_{\rm g}}$ . Let  $B_{\rm g}$  be a frame that is fixed to  $o_{\rm g}$  and has orthogonal unit vectors  $\hat{\imath}_{\rm g}$ ,  $\hat{\jmath}_{\rm g}$ , and  $\hat{k}_{\rm g}$ , where  $\hat{\imath}_{\rm g}$  is parallel to the leader's velocity vector  $p_{\rm g}$ , and the rotation matrix from  $B_{\rm g}$  to E is  $R_{\rm g}:[0,\infty)\to {\rm SO}(m)$ , which is assumed to be twice continuously differentiable.

This paper addresses the problem of formation control in the leader-fixed frame  $B_g$ . Let  $d_i \in \mathbb{R}^m$  be the desired position of  $o_i$  relative to  $o_g$  resolved in  $B_g$ . Thus, for all  $(i,j) \in \mathcal{P}, d_{ij} \triangleq d_i - d_j$  is the desired position of  $o_i$  relative to  $o_j$  resolved in  $B_g$ . Our objective is to design controls  $u_i$  and  $\Omega_i$  such that:

- (O1) For all  $(i, j) \in \mathcal{P}$ ,  $\lim_{t \to \infty} R_{\mathbf{g}}^{\mathbf{T}}(t)[q_i(t) q_j(t)] = d_{ij}$ .
- (O2) For all  $i \in \mathcal{I}$ ,  $\lim_{t \to \infty} [\dot{q}_i(t) \dot{q}_g(t) \dot{R}_g(t)d_i] = 0$ .
- (O3) For all  $i \in \mathcal{I}$ ,  $\lim_{t \to \infty} R_{\mathbf{g}}^{\Upsilon}(t)[q_i(t) q_{\mathbf{g}}(t)] = d_i$ .
- (O4) For all  $i \in \mathcal{I}$  and for all  $t \geq 0$ ,  $s_i(t) \in \mathcal{S}_i$ .

Objective (O1) states that the interagent positions approach the desired values. Objective (O2) states that each agent's velocity with respect to  $B_{\rm g}$  approaches the leader's velocity with respect to  $B_{\rm g}$ , and (O3) states that each agent approaches its desired relative position with the leader. Objective (O4) states that the agents' speed constraints are satisfied. If (O3) is satisfied, then (O1) is satisfied. However, we enumerate

these objectives independently because some results in this paper show that if no agents have access to a measurement of the leader's position, then (O1) is satisfied but (O3) is not.

Although the physical (i.e., frame-based) formulation of the formation control problem is described in three dimensions, the methods in this paper apply to all  $m \in \{2,3,4,\ldots\}$ . Thus, for the remainder of this paper, we consider the extended unicycle model (1)–(3) and the objectives (O1)–(O4), where  $m \in \{2,3,4,\ldots\}$ .

The interagent communication (i.e., feedback) structure is represented using an undirected graph. The agent index set  $\mathcal{I}$  is the *vertex set* of the graph, and the n elements of  $\mathcal{I}$  are the *vertices*. Let  $\mathcal{E} \subset \mathcal{I} \times \mathcal{I}$  be the *edge set*. The elements of  $\mathcal{E}$  are the *edges*. The graph  $\mathcal{G} = (\mathcal{I}, \mathcal{E})$  is *undirected* if for all  $(\ell_1, \ell_2) \in \mathcal{E}$ ,  $(\ell_2, \ell_1) \in \mathcal{E}$ . The graph  $\mathcal{G} = (\mathcal{I}, \mathcal{E})$  has a *walk of length l from*  $\ell_0 \in \mathcal{I}$  to  $\ell_l \in \mathcal{I}$  if there exists an (l+1)-tuple  $(\ell_0, \ell_1, \dots, \ell_l) \in \mathcal{I} \times \mathcal{I} \times \dots \times \mathcal{I}$  such that for all  $j \in \{1, 2, \dots, l\}$ ,  $(\ell_{j-1}, \ell_j) \in \mathcal{E}$ . The undirected graph  $\mathcal{G} = (\mathcal{I}, \mathcal{E})$  is *connected* if for all distinct  $i, j \in \mathcal{I}$ , there exists a walk from i to j.

Define the neighbor set  $\mathcal{N}_i \triangleq \{j \in \mathcal{I} : (j,i) \in \mathcal{E}\}$ . We assume that for all  $i \in \mathcal{I}, (i,i) \not\in \mathcal{E}$ , which implies that  $i \not\in \mathcal{N}_i$ . We assume that  $\mathcal{G} = (\mathcal{I}, \mathcal{E})$  is undirected and connected, and the ith agent has access to  $\{q_j\}_{j \in \mathcal{N}_i \cup \{i\}}$  and  $\{\dot{q}_j\}_{j \in \mathcal{N}_i \cup \{i\}}$  for feedback. In addition, we assume that each agent has access to measurements of the leader's velocity  $\dot{q}_g$ , the leader's acceleration  $\ddot{q}_g$ , and  $R_g$ ,  $\dot{R}_g$ , and  $\ddot{R}_g$ . However, we do not assume that all agents have access to a measurement of the leader's position  $q_g$ . In fact, the formation control algorithm in this paper only requires that at least one agent has access to a measurement of  $q_g$ .

# III. FORMATION CONTROL ALGORITHM

Consider  $\sigma: \mathbb{R}^m \to [0, \infty)$  defined by

$$\sigma(x) \triangleq 1/\sqrt{\nu_1 + \nu_2 ||x||^2},\tag{4}$$

where  $\nu_1, \nu_2 > 0$ , and  $\|\cdot\|$  is the 2-norm. Furthermore, consider  $\rho: \mathbb{R}^m \to \mathbb{R}^m$  defined by

$$\rho(x) \triangleq \sigma(x)x,\tag{5}$$

and note that  $\sup_{x\in\mathbb{R}^m}\|\rho(x)\|$  exists. Also, consider  $\rho':\mathbb{R}^m\to\mathbb{R}^{m\times m}$  defined by  $\rho'(x)\triangleq\partial\rho(x)/\partial x.$ 

Define the ith agent's desired velocity

$$p_{d,i} \triangleq \dot{q}_{g} + \dot{R}_{g}d_{i} - \alpha_{i}\rho(q_{i} - q_{g} - R_{g}d_{i})$$

$$+ \sum_{i \in \mathcal{N}_{i}} \beta_{ij}\rho(q_{j} - q_{i} + R_{g}d_{ij}),$$
(6)

where  $\alpha_i \geq 0$ , for all  $j \in \mathcal{N}_i$ ,  $\beta_{ij} = \beta_{ji} > 0$ , and for all  $j \notin \mathcal{N}_i$ ,  $\beta_{ij} = 0$ . It follows from (4) and (5) that all terms in (6) are bounded with the possible exception of the leader trajectory  $\dot{q}_{\rm g} + R_{\rm g}^{\rm T} d_i$ . The algorithm in this paper only requires that there exists  $l \in \mathcal{I}$  such that  $\alpha_l > 0$ , that is, at least one agent has access to a measurement of  $q_{\rm g}$ .

Define the desired speed

$$s_{\mathrm{d},i} \triangleq \|p_{\mathrm{d},i}\|. \tag{7}$$

Note that (O1)–(O3) along with (O4) cannot be achieved for an arbitrary leader trajectory  $\dot{q}_{\rm g} + \dot{R}_{\rm g}^{\rm T} d_i$ . Thus, we make the following assumption:

(A1) There exists  $\varepsilon > 0$  such that for all  $t \geq 0$ ,  $s_{d,i}(t) \in \mathcal{S}_{d,i} \triangleq (\underline{s}_i + \varepsilon, \overline{s}_i - \varepsilon)$ .

The next result provides sufficient conditions such that (A1) is satisfied. The proof is omitted for space considerations.

**Proposition 1.** Let  $\kappa_i > \varepsilon > 0$ . Assume that for  $t \geq 0$ ,  $\|\dot{q}_{\mathrm{g}}(t) + \dot{R}_{\mathrm{g}}(t)d_i\| \in (\underline{s}_i + \kappa_i, \bar{s}_i - \kappa_i)$ . Let  $\alpha_i \geq 0$  and  $\beta_{ij} \geq 0$  be such that  $\alpha_i + \sum_{j \in \mathcal{N}_i} \beta_{ij} < (\kappa_i - \varepsilon)/\sup_{x \in \mathbb{R}^m} \|\rho(x)\|$ . Then, for all  $q_i(0) \in \mathbb{R}^m$ , (A1) is satisfied.

Although Proposition 1 provides sufficient conditions on the leader trajectory and the gains  $\alpha_i$  and  $\beta_{ij}$  such that (A1) is satisfied, these conditions are not necessary. Thus, we invoke (A1), which can be satisfied either through the design in Proposition 1 or other means.

Next, define the time derivatives of  $p_{d,i}$  and  $s_{d,i}$  by

$$\dot{p}_{d,i} \triangleq \ddot{q}_{g} + \ddot{R}_{g}d_{i} - \alpha_{i}\rho'(q_{i} - q_{g} - R_{g}d_{i})(\dot{q}_{i} - \dot{q}_{g} - \dot{R}_{g}d_{i}) + \sum_{j \in \mathcal{N}_{i}} \beta_{ij}\rho'(q_{j} - q_{i} + R_{g}d_{ij})(\dot{q}_{j} - \dot{q}_{i} + \dot{R}_{g}d_{ij}), \quad (8)$$

$$\dot{s}_{\mathrm{d},i} \triangleq \frac{\partial s_{\mathrm{d},i}}{\partial p_{\mathrm{d},i}} \dot{p}_{\mathrm{d},i} = \frac{1}{s_{\mathrm{d},i}} p_{\mathrm{d},i}^{\mathrm{T}} \dot{p}_{\mathrm{d},i}. \tag{9}$$

To enforce the speed constraint (O4), we consider the speed barrier function  $h_i: \mathcal{S}_i \times \mathcal{S}_{d,i} \to (0,\infty)$  defined by

$$h_i(s_i, s_{d,i}) \triangleq \frac{(\bar{s}_i - s_{d,i})(s_{d,i} - \underline{s}_i)}{(\bar{s}_i - s_i)(s_i - \underline{s}_i)}.$$
 (10)

Furthermore, define

$$\frac{\partial h_i(s_i, s_{d,i})}{\partial s_i} \triangleq -\frac{(\bar{s}_i + \underline{s}_i - 2s_i)}{(\bar{s}_i - s_i)(s_i - \underline{s}_i)} h_i(s_i, s_{d,i}), \qquad (11)$$

$$\frac{\partial h_i(s_i, s_{d,i})}{\partial s_{d,i}} \triangleq \frac{(\bar{s}_i + \underline{s}_i - 2s_{d,i})}{(\bar{s}_i - s_i)(s_i - \underline{s}_i)}.$$
(12)

For notational convenience, we omit the arguments from (10)–(12) for the rest of the paper.

Then, the formation control is given by

$$u_{i} = \frac{-1}{g_{i}(s_{i}, R_{i})} \left[ f_{i}(s_{i}, R_{i}) + \left( \frac{1}{h_{i} + (s_{i} - s_{d,i}) \frac{\partial h_{i}}{\partial s_{i}}} \right) \times \left( \gamma_{i}(s_{i} - s_{d,i}) h_{i} + \left( (s_{i} - s_{d,i}) \frac{\partial h_{i}}{\partial s_{d,i}} - h_{i} \right) \dot{s}_{d,i} \right) \right],$$
(13)

$$\Omega_{i} = \eta_{i} s_{d,i} \left( R_{i}^{T} p_{d,i} v_{i}^{T} - v_{i} p_{d,i}^{T} R_{i} \right) 
+ \frac{1}{s_{d,i}^{2}} R_{i}^{T} \left( \dot{p}_{d,i} p_{d,i}^{T} - p_{d,i} \dot{p}_{d,i}^{T} \right) R_{i},$$
(14)

where  $\gamma_i > 0$  and  $\eta_i > 0$ . Since (A1) is satisfied, it follows that for all  $t \geq 0$ ,  $s_{\mathrm{d},i}(t) \in \mathcal{S}_{\mathrm{d},i}$ , which implies that  $\Omega_i$  is well defined. In the next section, we show that for all  $t \geq 0$ ,  $s_i(t) \in \mathcal{S}_i$ . Thus, the next result demonstrates that  $u_i$  is well defined. The proof is omitted for space considerations.

**Proposition 2.** For all  $(s_i, s_{d,i}) \in \mathcal{S}_i \times \mathcal{S}_{d,i}$ ,  $h_i + (s_i - s_{d,i})(\partial h_i/\partial s_i) > 0$ ; and  $h_i, \partial h_i/\partial s_{d,i}$ , and  $u_i$  are finite.

#### IV. STABILITY ANALYSIS

In this section, we analyze the closed-loop dynamics (1)–(14). Define the position error  $\zeta_i \triangleq q_i - q_g - R_g d_i$ . Differentiating  $\zeta_i$  and using (1) and (6) implies that

$$\dot{\zeta}_i = s_i R_i v_i - p_{d,i} - \alpha_i \rho(\zeta_i) + \sum_{j \in \mathcal{N}_i} \beta_{ij} \rho(\zeta_j - \zeta_i). \quad (15)$$

Consider the Lyapunov-like function  $V_0: \mathbb{R}^{mn} \to [0,\infty)$  defined by  $V_0(\{\zeta_i\}_{i\in\mathcal{I}}) \triangleq \sum_{i\in\mathcal{I}} \zeta_i^{\mathrm{T}} \zeta_i$ , and define  $\dot{V}_0(\{\zeta_i\}_{i\in\mathcal{I}}) \triangleq \sum_{i\in\mathcal{I}} \frac{\partial V_0}{\partial \zeta_i} \dot{\zeta}_i$ . The following preliminary result considers the case where the velocity  $s_i R_i v_i$  is a control variable, specifically,  $s_i R_i v_i = p_{\mathrm{d},i}$ . The proof is omitted for space considerations.

**Proposition 3.** Consider the closed-loop dynamics (15), which consists of (1) and (4)–(6), where  $s_i R_i v_i = p_{\mathrm{d},i}$ . Assume that  $\mathcal{G} = (\mathcal{I}, \mathcal{E})$  is undirected and connected. Then, the following statements hold:

i)  $\dot{V}_0$  is negative semidefinite, and  $\dot{V}_0$  is given by

$$\dot{V}_0(\{\zeta_i\}_{i\in\mathcal{I}}) = -\sum_{i\in\mathcal{I}} \left[ 2\alpha_i \sigma(\zeta_i) \|\zeta_i\|^2 + \sum_{j\in\mathcal{N}_i} \beta_{ij} \sigma(\zeta_i - \zeta_j) \|\zeta_i - \zeta_j\|^2 \right].$$
(16)

- ii) The equilibrium  $\{\zeta_i(t)\}_{i\in\mathcal{I}}\equiv 0$  of (15) is Lyapunov stable, and for all  $q_i(0)\in\mathbb{R}^m$ ,  $\zeta_i$  is bounded.
- iii) For all  $q_i(0) \in \mathbb{R}^m$ , (O1) and (O2) are satisfied.
- iv) If there exists  $l \in \mathcal{I}$  such that  $\alpha_l > 0$ , then  $\dot{V}_0$  is negative definite and for all  $q_i(0) \in \mathbb{R}^m$ , (O3) is satisfied.
- v) If (A1) is satisfied, then for all  $q_i(0) \in \mathbb{R}^m$ , (O4) is satisfied.

Proposition 3 shows that if  $s_i R_i v_i = p_{\mathrm{d},i}$  and there exists  $l \in \mathcal{I}$  such that  $\alpha_l > 0$  (i.e., at least one agent has a measurement of  $q_\mathrm{g}$ ), then (O1)–(O3) are satisfied, and if (A1) is satisfied, (O4) is satisfied. However, the speed  $s_i$  and pointing direction  $R_i v_i$  are not controls. Instead,  $s_i$  is determined from (2), which has control input  $u_i$ , and  $R_i v_i$  is determined from (3), which has control input  $\Omega_i$ . Before analyzing the full closed-loop dynamics (1)–(14), we examine the speed dynamics (2) and the associated control (13) to show that the speed constraint is satisfied.

Define the speed error  $\tilde{s}_i \triangleq s_i - s_{d,i}$ . Differentiating  $\tilde{s}_i$  and using (2) and (13) implies that

$$\dot{\tilde{s}}_{i} = \frac{-1}{h_{i} + \tilde{s}_{i} \frac{\partial h_{i}}{\partial s_{i}}} \left[ \gamma_{i} \tilde{s}_{i} h_{i} + \tilde{s}_{i} \left( \frac{\partial h_{i}}{\partial s_{d,i}} + \frac{\partial h_{i}}{\partial s_{i}} \right) \dot{s}_{d,i} \right]. \quad (17)$$

Consider the Lyapunov-like function  $Z_i: \mathbb{R} \to [0,\infty)$  defined by  $Z_i(\tilde{s}_i,s_{\mathrm{d},i}) \triangleq \frac{1}{2}h_i^2\tilde{s}_i^2$ , and define  $\dot{Z}_i(\tilde{s}_i,s_{\mathrm{d},i}) \triangleq \frac{\partial Z_i}{\partial \tilde{s}_i}\dot{\tilde{s}}_i + \frac{\partial Z_i}{\partial s_{\mathrm{d},i}}\dot{s}_{\mathrm{d},i}$ . The following result shows that that if (A1) is satisfied and  $s_i(0) \in \mathcal{S}_i$ , then for all  $t \geq 0$ ,  $s_i(t) \in \mathcal{S}_i$ . The proof is omitted for space considerations.

**Proposition 4.** Consider the closed-loop dynamics (17), which consists of (2) and (4)–(13), where (A1) is satisfied. Then, the following statements hold:

- i) For all  $(s_i, s_{\mathrm{d},i}) \in \mathcal{S}_i \times \mathcal{S}_{\mathrm{d},i}$ ,  $\dot{Z}_i(\tilde{s}_i, s_{\mathrm{d},i}) = -\gamma_i h_i^2 \tilde{s}_i^2 \le -\gamma_i a_i \tilde{s}_i^2$ , where  $a_i \triangleq 16\varepsilon^2/(\bar{s}_i \underline{s}_i)^2 > 0$ .
- ii) For all  $s_i(0) \in S_i$ , (O4) is satisfied.
- iii) For all  $s_i(0) \in S_i$ ,  $\lim_{t\to\infty} \tilde{s}_i(t) = 0$ .

Define the desired pointing direction  $b_{d,i} \triangleq p_{d,i}/s_{d,i}$ , and define the pointing direction error  $\tilde{b}_i \triangleq R_i v_i - b_{d,i}$ . Differentiating  $\tilde{b}_i$  and using (3) and (14) implies

$$\begin{split} \dot{\tilde{b}}_{i} &= \eta_{i} s_{\mathrm{d},i} \big( p_{\mathrm{d},i} v_{i}^{\mathrm{T}} v_{i} - R_{i} v_{i} p_{\mathrm{d},i}^{\mathrm{T}} R_{i} v_{i} \big) \\ &+ \frac{1}{s_{\mathrm{d},i}^{2}} \big( \dot{p}_{\mathrm{d},i} p_{\mathrm{d},i}^{\mathrm{T}} - p_{\mathrm{d},i} \dot{p}_{\mathrm{d},i}^{\mathrm{T}} \big) R_{i} v_{i} - \dot{b}_{\mathrm{d},i}. \end{split}$$

Since  $p_{\mathrm{d},i} = s_{\mathrm{d},i}b_{\mathrm{d},i}$ ,  $\dot{p}_{\mathrm{d},i} = \dot{s}_{\mathrm{d},i}b_{\mathrm{d},i} + s_{\mathrm{d},i}\dot{b}_{\mathrm{d},i}$ ,  $v_i^\mathrm{T}v_i = 1$ , and  $b_{\mathrm{d},i} = -\tilde{b}_i + R_iv_i$ , it follows that

$$\dot{\tilde{b}}_i = \eta_i s_{\mathrm{d},i}^2 \left( -\tilde{b}_i + \left( 1 - b_{\mathrm{d},i}^{\mathrm{T}} R_i v_i \right) R_i v_i \right) 
- \dot{b}_{\mathrm{d},i} \left( 1 - b_{\mathrm{d},i}^{\mathrm{T}} R_i v_i \right) - b_{\mathrm{d},i} \dot{b}_{\mathrm{d},i}^{\mathrm{T}} R_i v_i.$$

Since  $b_{\mathrm{d},i}$  is a unit vector, it follows that  $\dot{b}_{\mathrm{d},i}^{\mathrm{T}}b_{\mathrm{d},i}=0$ . In addition, note that  $1-b_{\mathrm{d},i}^{\mathrm{T}}R_{i}v_{i}=\frac{1}{2}\tilde{b}_{i}^{\mathrm{T}}\tilde{b}_{i}$  and  $R_{i}v_{i}=\tilde{b}_{i}+b_{\mathrm{d},i}$ . Thus,

$$\dot{\tilde{b}}_{i} = -\eta_{i} s_{\mathrm{d},i}^{2} \left( \tilde{b}_{i} - \frac{1}{2} \tilde{b}_{i}^{\mathrm{T}} \tilde{b}_{i} \left( \tilde{b}_{i} + b_{\mathrm{d},i} \right) \right) 
- \frac{1}{2} \dot{b}_{\mathrm{d},i} \tilde{b}_{i}^{\mathrm{T}} \tilde{b}_{i} - b_{\mathrm{d},i} \dot{b}_{\mathrm{d},i}^{\mathrm{T}} \tilde{b}_{i}.$$
(18)

Using (15) and  $s_i R_i v_i - p_{d,i} = \tilde{s}_i R_i v_i + s_{d,i} \tilde{b}_i$  implies

$$\dot{\zeta}_i = -\alpha_i \rho(\zeta_i) + \tilde{s}_i R_i v_i + s_{d,i} \tilde{b}_i + \sum_{j \in \mathcal{N}_i} \beta_{ij} \rho(\zeta_j - \zeta_i). \tag{19}$$

Next, define

$$Q \triangleq \{ (\{q_i\}_{i \in \mathcal{I}}, \{s_i\}_{i \in \mathcal{I}}, \{R_i\}_{i \in \mathcal{I}}) \in \mathbb{R}^{mn} \times \mathcal{S}_1 \times \dots \times \mathcal{S}_n \times SO(m)^n : \text{ for all } i \in \mathcal{I}, b_{d,i}^T(0)R_i(0)v_i \neq -1 \},$$

which is the set of initial conditions such that the angle from  $\dot{q}_i(0)$  to  $p_{\mathrm{d},i}(0)$  is not exactly  $\pi$  rad, and the initial speed is in the admissible range.

The next theorem is the main result, which shows that the equilibrium  $(\{\zeta_i(t)\}_{i\in\mathcal{I}}, \{\tilde{s}_i(t)\}_{i\in\mathcal{I}}, \{\tilde{b}_i(t)\}_{i\in\mathcal{I}}) \equiv (0,0,0)$  of the closed-loop system (17)–(19) is Lyapunov stable, for all initial conditions in  $\mathcal{Q}$ ,  $(\{\zeta_i(t)\}_{i\in\mathcal{I}}, \{\tilde{s}_i(t)\}_{i\in\mathcal{I}}, \{\tilde{b}_i(t)\}_{i\in\mathcal{I}})$  converges to zero, and (O1)–(O4) are satisfied. If the speed constraint is absent, then  $\mathcal{Q}$  consists of all initial conditions except those where the angle from  $\dot{q}_i(0)$  to  $p_{\mathrm{d},i}(0)$  is  $\pi$  rad. In this case, the closed-loop system is almost globally asymptotically stable. Note that topological constraints associated with  $\mathrm{SO}(m)$  prevent global asymptotic stability of the equilibrium using a continuous time-invariant control [37]. The proof is omitted for space considerations.

**Theorem 1.** Consider the closed-loop dynamics (17)–(19), which consists of (1)–(14), where (A1) is satisfied. Assume that  $\mathcal{G}=(\mathcal{I},\mathcal{E})$  is undirected and connected, and assume that there exists  $l\in\mathcal{I}$  such that  $\alpha_l>0$ . Then, the equilibrium  $(\{\zeta_i(t)\}_{i\in\mathcal{I}}, \{\tilde{s}_i(t)\}_{i\in\mathcal{I}}, \{\tilde{b}_i(t)\}_{i\in\mathcal{I}})\equiv (0,0,0)$  of (17)–(19) is Lyapunov stable. Furthermore, for all initial conditions  $(\{q_i(0)\}_{i\in\mathcal{I}}, \{s_i(0)\}_{i\in\mathcal{I}}, \{R_i(0)\}_{i\in\mathcal{I}})\in\mathcal{Q}$ , the

following statements hold:

- i) For all  $i \in \mathcal{I}$  and for all  $t \geq 0$ ,  $b_{\mathrm{d},i}^{\mathrm{T}}(t)R_i(t)v_i > -1$ .
- ii) For all  $i \in \mathcal{I}$ ,  $\lim_{t \to \infty} \zeta_i(t) = 0$ ,  $\lim_{t \to \infty} \tilde{s}_i(t) = 0$ , and  $\lim_{t \to \infty} \tilde{b}_i(t) = 0$ .
- iii) (O1)-(O4) are satisfied.

# V. HARDWARE PLATFORM

This section describes an experimental fixed-wing UAV platform. The UAV is equipped with a Pixhawk flight controller with the ArduPilot firmware, which provides attitude stabilization, waypoint navigation, and state estimation, and interfaces with a GPS receiver. An on-board Raspberry Pi single board computer obtains state estimates from the Pixhawk, communicates with other aircraft using WiFi, and runs the formation control algorithm (4)–(14).

We use the Skywalker X8 flying wing foam airframe, which consists of two wings attached to a fuselage section and reinforced with carbon fiber wing spars. A propeller and brushless motor are mounted to the aft end of the fuselage. The motor is spun by an electronic speed controller (ESC), producing thrust. The Pixhawk uses an extended Kalman filter to fuse measurements from a built-in 9-DOF IMU and barometer with the on-board GPS and airspeed sensor to estimate the position, attitude, and velocity of the UAV, as well as the wind velocity and calibration parameters of the on-board sensors. These estimates are used for stabilization and waypoint-based navigation, and are broadcast via a telemetry radio and shared with the Raspberry Pi via a USB connection.

For formation flight, the Pixhawk on each follower UAV is switched into Fly-By-Wire-A (FBWA) mode. In this mode, we provide three radio control (RC) override commands that simulate the pulse width modulation (PWM) signals that would be received from an RC transmitter operated by a human. The throttle PWM signal is passed directly to the ESC, and the Pixhawk maps the roll and pitch PWM signals linearly to desired attitude angles, where the minimum and maximum PWM values correspond to the minimum and maximum attitude angles stored in the Pixhawk. In this case, the minimum and maximum roll angles are  $\hat{\phi}_{\min,i} = -50 \deg$  and  $\hat{\phi}_{\max,i} = 50 \deg$ , and the minimum and maximum pitch angles are  $\hat{\theta}_{\min,i} = -20 \deg$  and  $\hat{\theta}_{\max,i} = 20 \deg$ .

# VI. FORMATION CONTROL IMPLEMENTATION

We apply the formation-control algorithm (4)–(14) to fixedwing UAVs, where  $v_i=e_1$  and  $\dot{\Omega}_{\rm g}$  is small enough to neglect for the control. Note that  $\alpha_i$  and  $\beta_{ij}$  can be generalized to diagonal  $m\times m$  matrices to allow independent tuning in the  $\hat{\imath}_{\rm E}$ ,  $\hat{\jmath}_{\rm E}$ , and  $\hat{k}_{\rm E}$  directions. For convenience in describing the rotation  $R_{\rm g}$ , let  $\psi_{\rm g}$ ,  $\theta_{\rm g}$ , and  $\phi_{\rm g}$  be the yaw, pitch, and roll Euler angles of a 3-2-1 rotation sequence which rotates E to  $B_{\rm g}$ . Thus,  $R_{\rm g}$  can be parameterized by  $\psi_{\rm g}$ ,  $\theta_{\rm g}$ , and  $\phi_{\rm g}$ . Similarly,  $R_i$  can be parameterized by  $\psi_i$ ,  $\theta_i$ , and  $\phi_i$ . Let  $\hat{\psi}_i$ ,  $\hat{\theta}_i$ , and  $\hat{\phi}_i$  denote the yaw, pitch, and roll of the aircraft. In the absence of wind and with angle-of-attack and side-slip angles equal to zero,  $\hat{\psi}_i = \psi_i$ ,  $\hat{\theta}_i = \theta_i$ , and  $\hat{\phi}_i = \phi_i$ . For compatibility with the control inputs and feedback presented

by the autopilot, we convert between the aircraft's angular velocity  $\Omega_i$  and the Euler angle derivatives  $\dot{\phi}_i$ ,  $\dot{\theta}_i$ ,  $\dot{\psi}_i$ .

The hardware platform described in Section V does not have the dynamics given by (1)–(3). However, we implement middle-loop controllers so the closed-loop UAV dynamics approximate the agent dynamics (1)–(3).

We use a PID controller with feedforward and anti-windup to command the pitch angle  $\hat{\theta}_{\mathrm{d},i}(t) \in [\hat{\theta}_{\min,i},\hat{\theta}_{\max,i}]$  such that the course angle  $\theta_i$  tracks the desired course angle  $\theta_{\mathrm{d},i} \triangleq \arcsin -e_3^\mathrm{T} p_{\mathrm{d},i}/s_{\mathrm{d},i}$ . The feedforward is  $\theta_{\mathrm{d},i}$ . Anti-windup is achieved by preventing the integrator state from changing if the pitch command  $\hat{\theta}_{\mathrm{d},i}$  is outside  $(\hat{\theta}_{\min,i},\hat{\theta}_{\max,i})$  and the pitch error  $\theta_i - \theta_{\mathrm{d},i}$  is such that integrating would drive  $\hat{\theta}_{\mathrm{d},i}$  further into saturation.

We use a PID controller with feedforward and anti-windup to command the roll angle  $\hat{\phi}_{\mathrm{d},i}(t) \in [\hat{\phi}_{\min,i},\hat{\phi}_{\max,i}]$  such that the course angle  $\psi_i$  tracks the desired course angle  $\psi_{\mathrm{d},i} \triangleq \mathrm{atan2}(e_2^\mathrm{T} p_{\mathrm{d},i}, e_1^\mathrm{T} p_{\mathrm{d},i})$ , where atan2 denotes the four-quadrant arctangent. Anti-windup is achieved in the same way as in the pitch controller. The feedforward is  $\arctan(\dot{\psi}_{\mathrm{d},i} s_i/g) \cos \hat{\theta}_i$ , where  $g = 9.81 \text{ m/s}^2$  is the acceleration due to gravity, and  $\arctan(\dot{\psi}_{\mathrm{d},i} s_i/g) \cos \hat{\theta}_i$  is the roll angle required to maintain a heading rate of  $\dot{\psi}_{\mathrm{d},i}$  at a speed of  $s_i$  based on the assumption of a coordinated turn. The feedforward is similar to that used in the ArduPlane L1 navigation controller and in [36].

To control the speed of the aircraft, we first convert the speed dynamics input  $u_i$  to a desired airspeed  $u_i' \triangleq u_i + s_{a,i} - s_i$ , where  $s_{a,i}$  is the measured airspeed. We then saturate  $u_i'$  to the flight envelope of the aircraft to obtain

$$u_i''(t) \triangleq \begin{cases} s_{\min,i} & u_i'(t) < s_{\min,i} \\ u_i'(t) & s_{\min,i} \le u_i'(t) \le s_{\max,i} \\ s_{\max,i} & u_i'(t) < s_{\max,i}, \end{cases}$$

where  $s_{\min,i}$  is the ARSPD\_FBW\_MIN parameter of the autopilot and  $s_{\mathrm{max},i}$  is the ARSPD\_FBW\_MAX parameter of the autopilot. We use a PID controller with feedforwar and anti-windup to command the throttle  $T_i(t) \in [0, 10]$ such that the airspeed  $s_{a,i}$  tracks  $u_i''$ . Thus, within the flig envelope,  $s_i$  tracks  $u_i$ . Anti-windup is achieved in in the san way as in the pitch and roll controllers. The feedforwar is  $T_0 + T_1(u_i'' - s_{0,i}) + T_\phi(\cos^{-2}\hat{\phi}_i - 1)$ , where  $T_0$  is the TRIM\_THROTTLE parameter of the autopilot,  $T_1 \ge 0$ ,  $s_{0,i}$ the TRIM\_ARSPD\_CM parameter of the autopilot converte to m/s,  $T_{\phi}$  is the TECS\_RLL2THR parameter of the autopile and  $T_{\phi}(\cos^{-2}\hat{\phi}_{i}-1)$  is an estimate of the additional thrott input required to maintain airspeed while turning. In practice,  $\dot{u}_i$ , and  $\dot{s}_i$  are estimated using backward Euler differentiation with a low-pass filter. The controller is tuned such that the speed dynamics from  $u_i$  to  $s_i$  approximate a first-order lowpass filter with pole at -0.4. Thus, these dynamics are (2), where  $f_i(R_i, s_i) = -0.4s_i$  and  $g_i(R_i, s_i) = 0.4$ .

The Raspberry Pi communicates with the Pixhawk via the DroneKit Python API and stores the state estimates, along with their timestamps in Python class instances. These instances are serialized using the cPickle library, compressed using zlib, and broadcast over the ad-hoc WiFi network via UDP at approximately 10 Hz.

#### VII. EXPERIMENTAL RESULTS AND DISCUSSION

This section describes a flight experiment using the multi-loop implementation described in Section VI and the hardware platform described in Section V. The experiment was conducted at the Lexington Model Airplane Club flying field located in Lexington, Kentucky on July 10, 2019. The wind was approximately 2 m/s from the southwest. Let n = 2 agents, and m = 3, and let  $f_i(s_i, R_i) =$  $-0.4s_i$  and  $g_i(s_i, R_i) = 0.4$ , which implies that the speed dynamics are a low-pass filter with unity gain at dc. The time constant 0.4 was estimated from the closed-loop step response of the UAV with the middle-loop speed controller. The desired positions are  $d_1 = \begin{bmatrix} -10 & 10 & 20 \end{bmatrix}^T$  m and  $d_2 = \begin{bmatrix} -10 & -10 & -20 \end{bmatrix}^T$  m. Let  $\alpha_i = \text{diag}(105, 105, 31.5)$ ,  $\beta_{12} = \beta_{21} = \text{diag}(50, 50, 15), \ \gamma_i = 1, \ \eta_i = 0.0003,$  $\nu_1=250000,\ \nu_2=1,\ \underline{s}_i=-\infty,\ \mathrm{and}\ \bar{s}_i=\infty,\ \mathrm{and}\ \mathrm{let}$  $T_{\rm s}=0.1~{\rm s}$  and  $\phi_{\rm g}(t)\equiv 0.$ 

After all UAVs have been launched, UAVs serving as agents are put into FBWA mode and formation-control is engaged using a switch on each agent's RC transmitter.

In this experiment, the leader UAV is commanded to follow a rectangular flight path. Figure 1 shows the UAVs trajectories, where the vertical axis is time. By  $t=40\,$  s, the UAVs have achieved the formation and stay in formation for the remainder of the experiment. Figure 2 shows the first rectangle in the trajectory from an overhead view. Figure 3 shows the relative position between the agents and the leader in the  $\hat{\imath}_{\rm E},\,\hat{\jmath}_{\rm E}$ , and

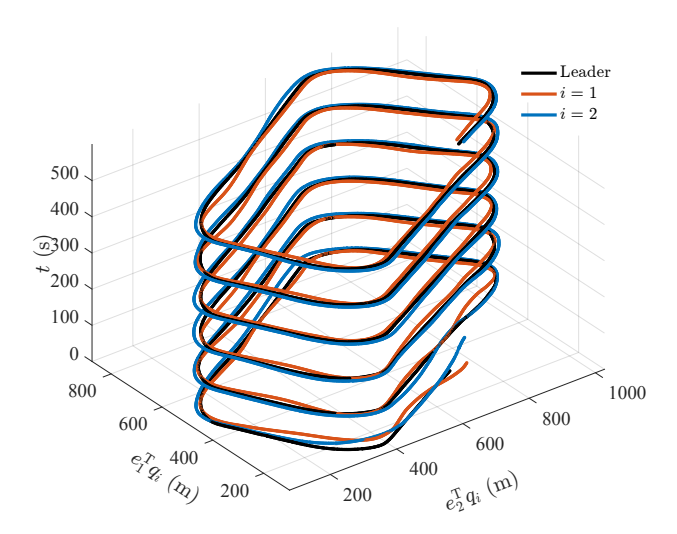


Fig. 1. Trajectories of leader and agents in the  $\hat{\imath}_{\rm E}-\hat{\jmath}_{\rm E}$  plane with time as the vertical axis. The agents converge to the desired relative positions at approximately  $t=40~\rm s.$ 

## REFERENCES

- G. Punzo, P. Karagiannakis, D. J. Bennet, M. Macdonald, and S. Weiss, "Enabling and exploiting self-similar central symmetry formations," *IEEE Trans. Aerosp. Electron. Syst.*, vol. 50, no. 1, pp. 689–703, 2014.
- [2] R. W. Beard, T. W. McLain, D. B. Nelson, D. Keingston, and D. Johnson, "Decentralized cooperative aerial surveillance using decentralized cooperative aerial surveillance using fixed-wing miniature UAVs," *Proc. IEEE*, vol. 94, no. 7, pp. 1306–1324, 2006.

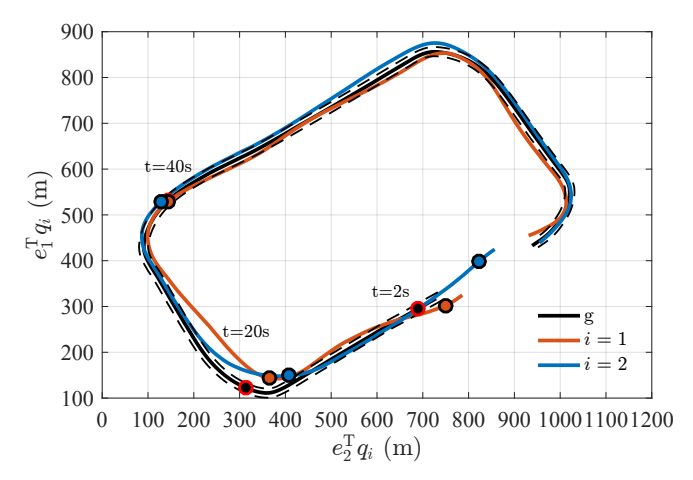


Fig. 2. Abbreviated trajectories of the leader and agents in the  $\hat{\imath}_{\rm E}-\hat{\jmath}_{\rm E}$  plane. The leader follows a rectangular trajectory and the agents converge to the desired positions.

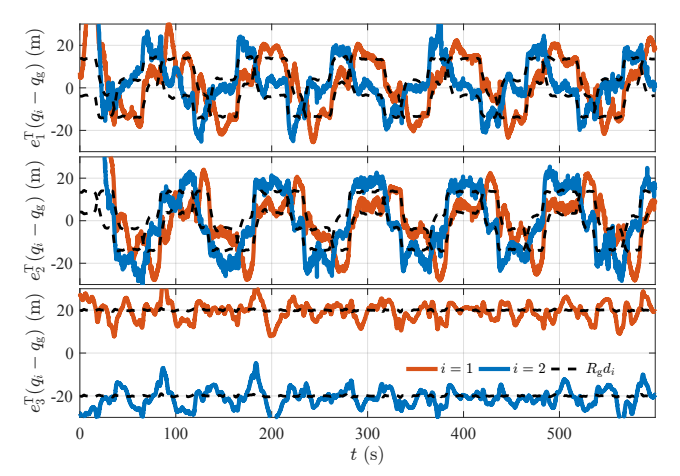


Fig. 3. Relative Position between the agents and the leader. The RMS of the norms of the position errors  $\|\zeta_i\|$  are 8.80 m and 8.87 m

- [3] G. Lafferriere, A. Williams, J. Caughman, and J. J. P. Veerman, "Decentralized control of vehicle formations," Syst. Contr. Lett., vol. 54, no. 9, pp. 899–910, 2005.
- [4] W. Ren, "On consensus algorithms for double-integrator dynamics," *IEEE Trans. Autom. Contr.*, vol. 53, no. 6, pp. 1503–1509, 2008.
- [5] Y. Cao and W. Ren, "Distributed coordinated tracking with reduced interaction via a variable structure approach," *IEEE Trans. Autom. Contr.*, vol. 57, no. 1, pp. 33–48, 2012.
- [6] Y. Cao and W. Ren, "Multi-vehicle coordination for double-integrator dynamics under fixed undirected/directed interaction in a sampled-data setting," Int. J. Robust Nonlinear Contr., vol. 20, pp. 987–1000, 2010.
- [7] Y. Gao and L. Wang, "Sampled-data based consensus of continuoustime multi-agent systems with time-varying topology," *IEEE Trans. Autom. Contr.*, vol. 56, no. 5, pp. 1226–1231, 2011.
- [8] H. G. Tanner, "Flocking with obstacle avoidance in switching networks of interconnected vehicles," in *Proc. IEEE Int. Conf. Robot. Automat.*, pp. 3006–3011, 2004.
- [9] B. J. Wellman and J. B. Hoagg, "A flocking algorithm with individual agent destinations and without a centralized leader," Sys. Contr. Lett., vol. 102, pp. 57–67, 2017.
- [10] D. Panagou, D. M. Stipanovi, and P. G. Voulgaris, "Distributed coordination control for multi-robot networks using Lyapunov-like barrier functions," *IEEE Trans. Autom. Contr.*, vol. 61, no. 3, pp. 617– 632, 2016.
- [11] R. Olfati-Saber, "Flocking for multi-agent dynamic systems: Algorithms and theory," *IEEE Trans. Autom. Contr.*, vol. 51, pp. 401–420, 2006.
- [12] D. V. Dimarogonas, S. G. Loizou, K. J. Kyriakopoulos, and M. M. Zavlanos, "A feedback stabilization and collision avoidance scheme for multiple independent non-point agents," *Automatica*, vol. 42, no. 2, pp. 229–243, 2006.
- [13] H. G. Tanner, A. Jadbabaie, and G. J. Pappas, "Flocking in fixed

- and switching networks," *IEEE Trans. Autom. Contr.*, vol. 52, no. 5, pp. 863–868, 2007.
- [14] D. Gu and Z. Wang, "Leader-follower flocking: Algorithms and experiments," *IEEE Trans. Contr. Sys. Tech.*, vol. 17, no. 5, pp. 1211– 1219, 2009.
- [15] H. Shi, L. Wang, and T. Chu, "Flocking of multi-agent systems with a dynamic virtual leader," *Int. J. Contr.*, vol. 82, no. 1, pp. 43–58, 2009.
- [16] H. Su, X. Wang, and Z. Lin, "Flocking for multi-agents with a virtual leader," *IEEE Trans. Autom. Contr.*, vol. 54, no. 2, pp. 293–307, 2009.
- [17] M. M. Zavlanos, M. B. Egerstedt, and G. J. Pappas, "Graph-theoretic connectivity control of mobile robot networks," *Proc. IEEE*, vol. 99, no. 9, pp. 1525–1540, 2011.
- [18] M. Guo, M. M. Zavlanos, and D. V. Dimarogonas, "Controlling the relative agent motion in multi-agent formation stabilization," *IEEE Trans. Autom. Contr.*, vol. 59, no. 3, pp. 820–826, 2014.
- [19] R. Olfati-Saber, J. A. Fax, and R. M. Murray, "Consensus and cooperation in networked multi-agent systems," *Proc. IEEE*, vol. 95, no. 1, pp. 215–233, 2007.
- [20] W. Ren, R. W. Beard, and E. M. Atkins, "Information consensus in multivehicle cooperative control," *IEEE Contr. Sys. Mag.*, vol. 27, no. 2, pp. 71–82, 2007.
- [21] Y. Cao, W. Yu, W. Ren, and G. Chen, "An overview of recent progress in the study of distributed multi-agent coordination," *IEEE Trans. Industrial Informatics*, vol. 9, no. 1, pp. 427–438, 2013.
- [22] Y. Gu, B. Seanor, G. Campa, M. R. Napolitano, L. Rowe, S. Gururajan, and S. Wan, "Design and flight testing evaluation of formation control laws," *IEEE Trans. Contr. Sys. Tech.*, vol. 14, pp. 1105–1112, 2006.
- [23] M. Turpin, N. Michael, and V. Kumar, "Trajectory design and control for aggressive formation flight with quadrotors," *Autonomous Robots*, vol. 33, pp. 143–156, 2012.
- [24] C. Park, N. Cho, K. Lee, and Y. Kim, "Formation flight of multiple UAVs via onboard sensor information sharing," *Sensors*, vol. 15, pp. 17398–17419, 2015.
- [25] S. Mao, W. K. Tan, and K. H. Low, "Autonomous formation flight of indoor UAVs based on model predictive control," in AIAA Infotech@ Aerospace, p. 515, 2016.
- [26] V. Darbari, S. Gupta, and O. P. Verma, "Dynamic motion planning for aerial surveillance on a fixed-wing UAV," in *Proc. Int. Conf. Unmanned Aircrat Systems*, (Miami, FL), pp. 488–497, June 2017.
- [27] H. G. de Marina, Z. Sun, M. Bronz, and G. Hattenberger, "Circular formation control of fixed-wing UAVs with constant speeds," in *Proc. IEEE/RSJ Int. Conf. Intelligent Robots and Sys.*, (Vancouver, Canada), pp. 5298–5303, September 2017.
- [28] B. J. Wellman and J. B. Hoagg, "Sampled-data flocking with application to unmanned rotorcraft," in *Proc. AIAA Guid. Nav. Contr. Conf.*, AIAA-2018-1856, (Kissimmee, FL), January 2018.
- [29] C. Heintz, S. C. Bailey, and J. B. Hoagg, "Formation control of fixed-wing unmanned aircraft: Theory and experiments," in *Proc. AIAA Guid. Nav. Contr. Conf.*, AIAA-2019-1168, (San Diego, CA), January 2019.
- [30] D. M. Stipanovi, G. Inalhan, R. Teo, and C. J. Tomlin, "Decentralized overlapping control of a formation of unmanned aerial vehicles," *Automatica*, vol. 40, no. 8, pp. 1285–1296, 2004.
- [31] C. B. Low, "A dynamic virtual structure formation control for fixed-wing UAVs," in *Proc. IEEE Int. Conf. Contr. Automation*, (Santiago, Chile), pp. 627–632, December 2011.
- [32] M. Zhang and H. H. T. Liu, "Formation flight of multiple fixed-wing unmanned aerial vehicles," in *Proc. Amer. Contr. Conf.*, (Washington, D.C.), pp. 1614–1619, June 2013.
- [33] C. Heintz and J. B. Hoagg, "Formation control in a leader-fixed frame for agents with extended unicycle dynamics that include orientation kinematics on SO(m)," in *Proc. IEEE Conf. Decision Contr.*, pp. 8230– 8235, 2019.
- [34] T. D. Barfoot and C. M. Clark, "Motion planning for formations of mobile robots," *Robotics Auton. Sys.*, vol. 46, pp. 65–78, 2004.
- [35] C. B. Low and D. Wang, "Gps-based tracking control for a car-like wheeled mobile robot with skidding and slipping," *IEEE/ASME Trans. Mechatronics*, vol. 13, no. 4, pp. 480–484, 2008.
- [36] R. W. Beard, J. Ferrin, and J. Humpherys, "Fixed wing uav path following in wind with input constraints," *IEEE Transactions on Control Systems Technology*, vol. 22, pp. 2103–2117, Nov 2014.
- [37] S. P. Bhat and D. S. Bernstein, "A topological obstruction to continuous global stabilization of rotational motion and the unwinding phenomenon," Sys. Contr. Lett., vol. 39, no. 1, pp. 63 70, 2000.